Journal of the Physical Society of Japan
Vol. 78, No. 1, January, 2009, 014708

Sign Reversal of AC Josephson Current in a Ferromagnetic Josephson Junction

Shin-ichi HIKINO[1], Michiyasu MORI[1,2], Saburo TAKAHASHI[1,2], and Sadamichi MAEKAWA[1,2]

[1]*Institute for Materials Research, Tohoku University, Sendai 980-8577*
[2]*CREST, Japan Science and Technology Agency, Tokyo 102-0075*

(Received September 9, 2008; accepted November 4, 2008; published January 13, 2009)

The ac Josephson effect in a ferromagnetic Josephson junction, which is composed of two superconductors separated by a ferromagnetic metal (FM), is studied by a tunneling Hamiltonian and Green's function method. We obtain two types of superconducting phase dependent currents, i.e., Josephson current and quasiparticle-pair-interference current (QPIC). These currents change their signs with thickness of the FM layer due to the 0–π transition characteristic to the ferromagnetic Josephson junction. As a function of applied voltage, the Josephson critical current shows a logarithmic divergence called the Riedel peak at the gap voltage, while the QPIC shows a discontinuous jump. The Riedel peak reverses due to the 0–π transition and disappears near the 0–π transition point. The discontinuous jump in the QPIC also represents similar behaviors to the Riedel peak. These results are in contrast to the conventional ones.

KEYWORDS: ac Josephson effect, Riedel peak, ferromagnetic Josephson junction, superconductor, ferromagnet, 0-state, pi-state
DOI: 10.1143/JPSJ.78.014708

1. Introduction

The Josephson effect is a macroscopic quantum phenomenon involving phase coherence between two superconductors (SC's), and is characterized by a zero voltage current through a thin insulating barrier (dc Josephson effect). On the other hand, when a finite voltage is applied across the junction, an alternating current flows according to time-dependence of phase-difference, θ, in two superconductors (ac Josephson effect), which gives two types of current as, $I_{J1} = I_{c1} \sin\theta$ and $I_{J2} = I_{c2} \cos\theta$.[1)] The former is the same as the dc Josephson current except for time-dependence of θ, while the latter is a phase-dependent dissipative current inherent to the ac case. As a function of applied voltage, V, the amplitudes, I_{c1} and I_{c2}, show singularities originating from the gap, Δ, in an s-wave superconductor. The I_{c1} has a logarithmic divergence called the Riedel peak at the gap voltage, $V = 2\Delta/e$, due to the square root singularities in the density of states,[2–7)] while the I_{c2} shows a discontinuity at $V = 2\Delta/e$ and is zero below $V < 2\Delta/e$ at zero temperature.[3,5)] The I_{c2} is experimentally observed near the superconducting transition temperature, T_c,[8)] in various types of Josephson junctions.[9–14)]

Recently, a Josephson junction with a ferromagnetic metal (FM), which is called the ferromagnetic Josephson junction, has been actively studied both experimentally and theoretically.[15–28)] One of the most interesting phenomena in the ferromagnetic Josephson junction is the oscillation of the I_{c1} as a function of the thickness of the ferromagnetic film. The mechanism of the oscillation is similar to that of Fulde–Ferrell–Larkin–Ovchinnikov (FFLO) state.[29,30)] Cooper pairs penetrating into the FM acquire a finite center of mass momentum proportional to the magnetic exchange splitting, h_{ex}, between up- and down-spin bands. As a result, the pair correlation in FM oscillates as a function of the thickness of FM. If the thickness of the FM is about a half of the period of the oscillation, the current-phase relation is shifted by π from that of a conventional Josephson junction (0-junction) like as, $I_{c1} < 0$. This is called a π-junction, which has potential applications as a quantum bit.[31,32)] In addition, the π-junction is used in some experiments to measure a nonsinusoidal current-phase relation. Using the ac Josephson effect, Sellier *et al.* experimentally evidenced the second harmonic term given by $\sin 2\theta$ in the SC/FM/SC junction.[20)] However, most of studies on the π junctions have been so far focused on the dc Josephson effect. Studies on the ac Josephson effect in ferromagnetic π junctions will open a new pathway of basic physics and will contribute to realize the quantum bit including SC/FM/SC junctions.

In this paper, we study the ac Josephson effect in a SC/X/SC junction, where X is either a NM or a FM. Using a tunneling Hamiltonian and Green's function method,[33–35)] we obtain two types of phase dependent current, i.e. the ac Josephson current ($I_{J1} = I_{c1} \sin\theta$) and the QPIC ($I_{J2} = I_{c2} \cos\theta$). In a SC/NM/SC junction, I_{c1} and I_{c2} monotonously decrease with the thickness of NM. As a function of applied voltage, I_{c1} shows a logarithmic divergence (the Riedel peak) at the gap voltage, $V = 2\Delta/e$, while I_{c2} discontinuously jumps at the same voltage. On the other hand, in a SC/FM/SC junction, I_{c1} and I_{c2} exhibit the strong dependence on the thickness of FM and change their signs by crossing the 0–π transition point due to the magnetic exchange splitting between the up- and down-spin bands in FM. In particular, it is predicted that the Riedel peak in I_{c1} disappears at the 0–π transition and the 0–π transition occurs in I_{c2} like as I_{c1}.

The rest of this paper is organized as follows. In §2, we introduce the model Hamiltonian including the tunneling Hamiltonian, and explain the formulation to calculate the ac current by the thermal Green's function method. In §3, the ac Josephson current and the QPIC in the SC/NM/SC and SC/FM/SC junctions are shown as functions of thickness and applied voltage. We compare these two types of junctions and discuss similarities and differences. Summary and discussion are given in §4. Below, $\hbar = 1$ and $k_B = 1$ are used in the equations.

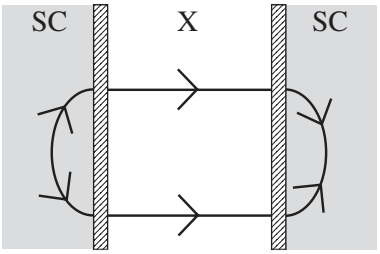

Fig. 1. Fourth order diagram with a tunneling matrix element contributing to I_J. Insulating barrier is at interfaces between SC and X.

2. Tunneling Hamiltonian Approach for AC Josephson Current

2.1 Model Hamiltonian

We consider a junction composed of a ballistic FM with the thickness d and s-wave SC electrodes as shown in Fig. 1. A dc bias voltage, V, is applied across the junction.

The SCs and the FM are connected by tunneling Hamiltonian. The total Hamiltonian is given by

$$H = H_{\rm SC}^{\rm L} + H_{\rm SC}^{\rm R} + H_{\rm FM} + H_{\rm T}, \tag{1}$$

$$H_{\rm SC}^{\rm L} = \sum_\sigma \int {\rm d}\boldsymbol{r}\, \psi_{{\rm L},\sigma}^\dagger \left(-\frac{1}{2m}\nabla^2 - \mu\frac{eV}{2}\right)\psi_{{\rm L},\sigma} + \Delta {\rm e}^{{\rm i}\theta_{\rm L}} \int {\rm d}\boldsymbol{r}\, \psi_{{\rm L},\uparrow}^\dagger \psi_{{\rm L},\downarrow}^\dagger + {\rm h.c.}, \tag{2}$$

$$H_{\rm SC}^{\rm R} = \left({\rm L} \to {\rm R}, -\mu\frac{eV}{2} \to +\mu\frac{eV}{2}\right), \tag{3}$$

$$H_{\rm FM} = \sum_\sigma \int {\rm d}\boldsymbol{r}\, \psi_{{\rm FM},\sigma}^\dagger \left(-\frac{1}{2m}\nabla^2 - \mu - {\rm i}\sigma h_{\rm ex}\right)\psi_{{\rm FM},\sigma}, \tag{4}$$

$$H_{\rm T} = \sum_\sigma \int_{\boldsymbol{r}\in{\rm L},\boldsymbol{r}'\in{\rm FM}} {\rm d}\boldsymbol{r}\, {\rm d}\boldsymbol{r}'\, T_{\boldsymbol{r},\boldsymbol{r}'} \psi_{{\rm L},\sigma}^\dagger \psi_{{\rm FM},\sigma} + \sum_\sigma \int_{\boldsymbol{r}\in{\rm R},\boldsymbol{r}'\in{\rm FM}} {\rm d}\boldsymbol{r}\, {\rm d}\boldsymbol{r}'\, T_{\boldsymbol{r},\boldsymbol{r}'} \psi_{{\rm R},\sigma}^\dagger \psi_{{\rm FM},\sigma} + {\rm h.c.}, \tag{5}$$

where $\psi_{i,\sigma} \equiv \psi_{i,\sigma}(\boldsymbol{r})$ is the electron field operator with the position $\boldsymbol{r}$ in the region i (= L, R, or FM) and the spin σ (= $\uparrow, \downarrow$). We adopt the BCS mean field Hamiltonian $H_{\rm SC}^{\rm L(R)}$ with the s-wave gap Δ and the phase variable $\theta_{\rm L(R)}$ in the left (right) SC. Then, the phase difference is given by $\theta \equiv \theta_{\rm L} - \theta_{\rm R}$. The electron mass and the chemical potential are denoted by m and μ, respectively. Note that $\mp eV/2$ is added in the Hamiltonian (2), since the applied voltage, V, imposes a chemical potential difference, $V/2$, at each boundary between FM and SC. The Hamiltonian of the FM, $H_{\rm FM}$, which has no impurity scattering, has the exchange energy, $h_{\rm ex}$. $H_{\rm T}$ is the tunneling Hamiltonian, whose matrix element is denoted by $T_{\boldsymbol{r},\boldsymbol{r}'}$ and has a finite value at the SC/FM boundary as, $T_{\boldsymbol{r},\boldsymbol{r}'} = T_0\delta(\boldsymbol{r}-\boldsymbol{r}')\delta(\boldsymbol{r}-\boldsymbol{r}_{\rm L(R)})$. $\boldsymbol{r}_{\rm L(R)}$ is the position of the interface between the left (right) SC and the FM.

We calculate the expectation value of a current operator,

$$\hat{J} = -{\rm i}e \sum_\sigma \int_{\boldsymbol{r}\in{\rm L},\boldsymbol{r}'\in{\rm FM}} {\rm d}\boldsymbol{r}\, {\rm d}\,\boldsymbol{r}' T_{\boldsymbol{r},\boldsymbol{r}'} {\rm e}^{-{\rm i}eVt/2} \psi_{{\rm L},\sigma}^\dagger(x)\psi_{{\rm FM},\sigma}(x') + {\rm h.c.}, \tag{6}$$

where x involves both time, t, and $\boldsymbol{r}$. The superconducting phase dependent current is given by

$$I_{\rm J} \equiv \langle \hat{J} \rangle = I_{\rm c1}\sin\theta + I_{\rm c2}\cos\theta, \tag{7}$$

where $\langle \hat{J} \rangle$ is the expectation value of the current operator. The first term of eq. (7) is the Josephson current and $I_{\rm c1}$ is the Josephson critical current. The second term is called the quasiparticle-pair-interference current (QPIC).

2.2 Josephson critical current and QPIC formula

In the SC/FM/SC junction, the fourth order term of $\hat{J}$ with regard to $T_{\boldsymbol{r},\boldsymbol{r}'}$ is shown in Fig. 1. Detailed calculations are given in Appendices A and B. For $h_{\rm ex}/\mu$, $\omega_n/\mu \ll 1$, and temperature, $T = 0\,{\rm K}$, $I_{\rm c1}$ and $I_{\rm c2}$ are given by,

$$I_{\rm c1} = \frac{\sigma_0\Delta_0^2}{\pi e}\int_{\Delta_0}^\infty {\rm d}E \frac{\Theta(\Delta_0 - |E-eV|)}{\sqrt{E^2-\Delta_0^2}\sqrt{\Delta_0^2-(E-eV)^2}} \times \left\{ {\rm Ci}\left(\frac{2E-eV}{v_{\rm F}}d\right)\sin\left(\frac{2E-eV}{v_{\rm F}}d\right) - \cos\left(\frac{2E-eV}{v_{\rm F}}d\right)\left[{\rm Si}\left(\frac{2E-eV}{v_{\rm F}}d\right) - \frac{\pi}{2}\right]\right\} \times \cos\left(\frac{2h_{\rm ex}}{v_{\rm F}}d\right), \tag{8}$$

$$I_{\rm c2} = \frac{\sigma_0\Delta_0^2}{e}\int_0^{eV/2-\Delta_0} {\rm d}E \times \frac{\Theta(eV-2\Delta_0)}{\sqrt{(E+eV/2)^2-\Delta_0^2}\sqrt{(E-eV/2)^2-\Delta_0^2}} \times \cos\left(\frac{2E}{v_{\rm F}}d\right)\cos\left(\frac{2h_{\rm ex}}{v_{\rm F}}d\right), \tag{9}$$

where Δ_0 is the superconducting gap at $T = 0\,{\rm K}$, $\sigma_0 \equiv 16\pi e^2 T_0^4 N_{\rm L}(0)N_{\rm R}(0)[mv/(2\pi d)]^2$ is a constant determined by materials and interface, $N_{\rm L(R)}$ is the density of states in the left (right) lead at the Fermi level, $v_{\rm F}$ is the Fermi velocity, v and d are the volume and the thickness of the X, respectively. ${\rm Ci}(x)$ and ${\rm Si}(x)$ are the cosine and sine integrals, respectively. When $h_{\rm ex} = 0$, our formulation reproduces the current in the SC/NM/SC junction.

For $d/\xi_0 \gg 1$, eq. (8) is simplified as

$$I_{\rm c1} \simeq \frac{\sigma_0\Delta_0^2}{\pi e}\int_{\Delta_0}^\infty {\rm d}E \frac{\Theta(\Delta_0 - |E-eV|)}{\sqrt{E^2-\Delta_0^2}\sqrt{\Delta_0^2-(E-eV)^2}} \times \cos\left(\frac{2h_{\rm ex}}{v_{\rm F}}d\right)\frac{v_{\rm F}}{2E-eV}\frac{1}{d}, \tag{10}$$

where $\xi_0 \equiv v_{\rm F}/2\Delta_0$. It is found that $I_{\rm c1}$ decays with d in the power law as $1/d$. This behavior is consistent with the case of dc Josephson critical current in a double barrier Josephson junction.[28] On the other hand, for $d \to 0$, eqs. (8) and (9) reproduce the current in SC/I/SC junctions.[5] The integration in eqs. (8) and (9) is numerically carried out and results are shown in the next section.

3. d- and V-Dependence of $I_{\rm c1}$ and $I_{\rm c2}$

In this section, we show thickness d and bias voltage V dependences of $I_{\rm c1}$ and $I_{\rm c2}$. First, the SC/NM/SC junction is discussed to see the difference between NM and FM cases clearly. Then, we will give detailed discussions on the SC/FM/SC junction.

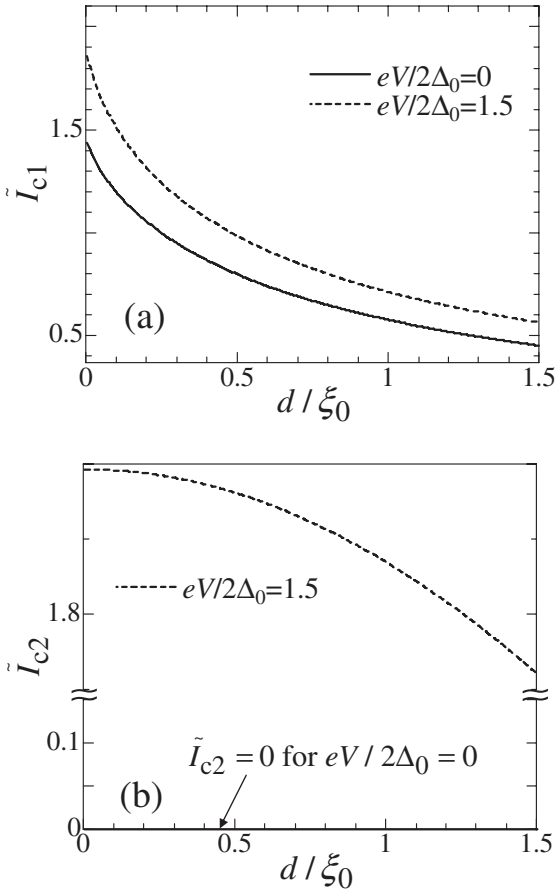

Fig. 2. (a) Normalized Josephson critical current, $\tilde{I}_{c1}$, and (b) the quasiparticle-pair-interference current, $\tilde{I}_{c2}$, as functions of d/ξ_0 for a SC/NM/SC junction ($h_{ex}=0$), where $\tilde{I}_{c1}=I_{c1}\pi e/\sigma_0\Delta_0$ and $\tilde{I}_{c2}=I_{c2}\pi e/\sigma_0\Delta_0$.

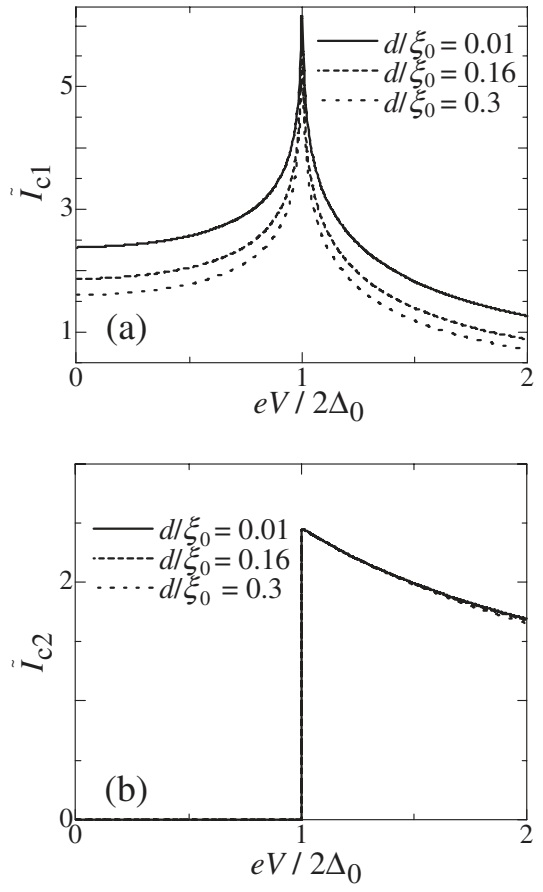

Fig. 3. (a) Normalized Josephson critical current, $\tilde{I}_{c1}$, and (b) quasiparticle-pair-interference current, $\tilde{I}_{c2}$, as functions of $eV/2\Delta_0$ in a SC/NM/SC junction, where $\tilde{I}_{c1}=I_{c1}\pi e/\sigma_0\Delta_0$ and $\tilde{I}_{c2}=I_{c2}\pi e/\sigma_0\Delta_0$.

3.1 SC/NM/SC junction

The thickness dependence of I_{c1} and I_{c2} is shown for several values of V in Fig. 2. In Fig. 2(a), the vertical axis is the normalized I_{c1} and the horizontal axis is the thickness d normalized by the coherence length ξ_0. It is found that I_{c1} shows a monotonic decrease as a function of d. For $d/\xi_0 \gg 1$, I_{c1} decreases in the power law as $1/d$ shown in eq. (10). In Fig. 2(b), I_{c2} is plotted. It is found that I_{c2} decreases as a function of d for $eV/2\Delta_0=1.5$, while it is always equal to zero at $eV/2\Delta_0=0$.

The I_{c1} in the SC/NM/SC junction is shown for several values of d in Fig. 3(a). The vertical axis is the normalized I_{c1} and the horizontal axis is the normalized voltage, $eV/2\Delta_0$. In Fig. 3(a), I_{c1} shows the Riedel peak at the gap voltage similar to that in a SC/I/SC junction. In this system, the Riedel peak exhibits weak dependence on d. The I_{c2} is shown in Fig. 3(b). It is found that I_{c2} has discontinuity at $eV/2\Delta_0=1$. The behavior of I_{c2} is the same as the case of SC/I/SC and I_{c2} exhibits very weak dependence on d.

Here, we examine the above results in details. I_{c1} shows the monotonic decrease as a function of d, which represents a decoherence of the Cooper pair penetrating into the NM. This behavior is equivalent to the case of dc Josephson effect. On the other hand, the behavior of I_{c2} is quite different from that of I_{c1}, since I_{c2} has a finite value only when V is larger than the gap voltage as shown by Fig. 3(b). Therefore, it is interpreted as quasiparticles in the band below the superconducting gap contribute to I_{c2} and carry the superconducting phase coherent dissipative current as in the case of a SC/I/SC junction.[36] Moreover, I_{c2} in a long SC/NM/SC junction ($d \gg \xi_0$) oscillates as a function of d and V with the period $(4\pi E/v_F)d$ because of $\cos[(2E/v_F)/d]$ in eq. (9). This behavior represents the phase shift by π and the 0–π transition occurs as a function of d and V. In the V-dependence of I_{c1}, the divergence of I_{c1} at the gap voltage is also shown in the SC/I/SC junctions. Since, the density of states has a square-root singularity at the gap edge as we can see in eq. (8), the amplitude of the Josephson critical current produces a logarithmic singularity at the gap voltage. This mechanism on the singularity is the same as that of SC/I/SC junction. In I_{c2}, the current vanishes for $eV/2\Delta_0<1$ and jumps at the $eV/2\Delta_0=1$. This behavior is similar to that of the SC/I/SC junctions. In a long SC/NM/SC junction ($d \gg \xi_0$), I_{c2} oscillates as a function of V with the period $(4\pi E/v_F)d$ as shown in eq. (9).

3.2 SC/FM/SC junction

In this subsection, the case of the SC/FM/SC junction is compared with that of the SC/NM/SC junction from the viewpoints of the d-dependences of I_{c1} and I_{c2} as shown in Fig. 4. In Fig. 4(a), the normalized I_{c1} is plotted as a function of d/ξ_0. For $eV/2\Delta_0=0$, i.e., dc Josephson effect, I_{c1} shows a damped oscillatory behavior as a function of d and the 0–π transition occurs by increasing d unlike the case of SC/NM/SC junction. For $eV/2\Delta_0=1.5$, I_{c1} is qualita-

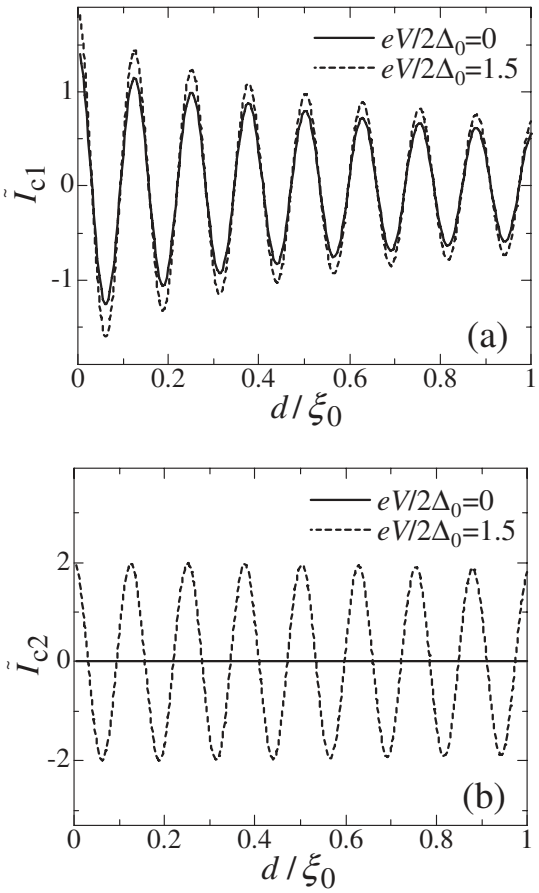

Fig. 4. (a) Normalized Josephson critical current, $\tilde{I}_{c1}$, and (b) quasiparticle-pair-interference current, $\tilde{I}_{c2}$, as functions of d/ξ_0 for $h_{ex}/\Delta_0 = 50$ in SC/FM/SC junction, where $\tilde{I}_{c1} = I_{c1}\pi e/\sigma_0\Delta_0$ and $\tilde{I}_{c2} = I_{c2}\pi e/\sigma_0\Delta_0$.

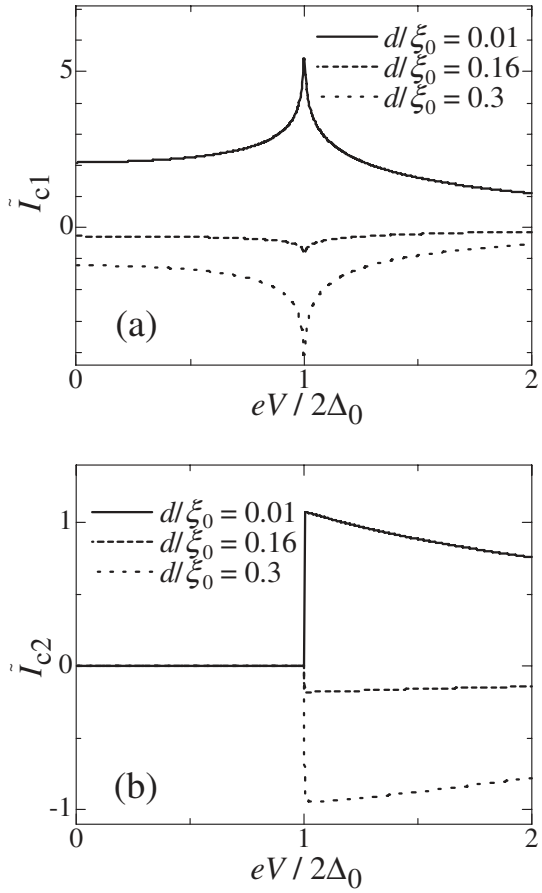

Fig. 5. (a) Normalized Josephson critical current, $\tilde{I}_{c1}$, and (b) quasiparticle-pair-interference current, $\tilde{I}_{c2}$, as functions of $eV/2\Delta_0$ for $h_{ex}/\Delta_0 = 50$ in SC/FM/SC junction, where $\tilde{I}_{c1} = I_{c1}\pi e/\sigma_0\Delta_0$ and $\tilde{I}_{c2} = I_{c2}\pi e/\sigma_0\Delta_0$.

tively the same as that in the dc Josephson effect. On the other hand, I_{c2} is zero for $eV/2\Delta_0 = 0$, but has a finite value for $eV/2\Delta_0 = 1.5$ similar to the SC/NM/SC junction. However, the I_{c2} changes its sign with increasing d due to the 0–π transition and vanishes at the transition point as shown in Fig. 4(b).

Figure 5 shows the ac current amplitude as a function of V in the SC/FM/SC junction. In Fig. 5(a), the vertical axis is the normalized I_{c1} and the horizontal axis is the normalized voltage, $eV/2\Delta_0$. In this system, the Riedel peak exhibits a strong dependence on d and changes its sign with increasing d due to the 0–π transition. Therefore, near the thickness at which the 0–π transition occurs, the Riedel peak disappears as shown in Fig. 5(a). In Fig. 5(b), it is found that I_{c2} has a finite value above $eV/2\Delta_0 = 1$. For $d/\xi_0 = 0.01$, the behavior of I_{c2} is the same as those of SC/I/SC and SC/NM/SC junctions. On the other hand, I_{c2} changes its sign with increasing d due to the 0–π transition and disappears near the thickness at which the 0–π transition occurs, as shown in Fig. 5(b).

The I_{c1} shows the damped oscillatory behavior as a function of d and the 0–π transition occurs. In eq. (8), only the ratio of h_{ex} and v_F determines the period of oscillation in the I_{c1}–d curve. The mechanism of 0–π transition in the ac Josephson effect is the same as that of the 0–π transition in the dc Josephson effect. Concerning I_{c2}, it has a finite value above $eV/2\Delta_0 = 1$, similar to the SC/I/SC and SC/NM/SC junctions. The behavior of I_{c2} is quite different from that of SC/NM/SC junction. In the SC/FM/SC junction, the oscillating term in eq. (9) is composed of two part. One is $\cos(2Ed/v_F)$ (the region of E being from 0 to $eV/2 - \Delta_0$), the other is $\cos(2h_{ex}d/v_F)$. In the practical case, h_{ex} is experimentally larger than eV.[17–27] Therefore, the period is dominated by h_{ex} and is short compared with ξ_0. The V-dependence of I_{c1} and I_{c2} in the SC/FM/SC junction shows remarkable phenomenon. In I_{c1}, the Riedel peak exhibits a strong dependence on d. It changes its sign with changing d and disappears at the 0–π transition point as shown in Fig. 6(a). I_{c2} also changes its sign with changing d and disappears at the 0–π transition point as shown in Fig. 6(b). We expect that these results provide a new method to observe the 0–π transition in SC/FM/SC junctions.

We take a look at the total ac current given by

$$I = \sqrt{I_{c1}^2 + I_{c2}^2}\,\sin(2eVt + \chi), \tag{11}$$

$$\chi = \arctan(I_{c2}/I_{c1}). \tag{12}$$

Figure 6 shows the current-phase relation (CPR) for $h_{ex}/\Delta_0 = 100$, $d/\xi_0 = 0.07$, and $eV/\Delta_0 = 1.5$ and 2.5. For $eV/2\Delta_0 < 1$, only the Josephson current flows because of $I_{c2} = 0$. Therefore, the CPR represents a conventional behavior as in a SC/I/SC junction as shown by the dashed line in Fig. 6. On the other hand, for $eV/2\Delta_0 > 1$, the phase of CPR is shifted by χ due to the finite QPIC. The behavior is shown in the solid line in Fig. 6. From these results, we

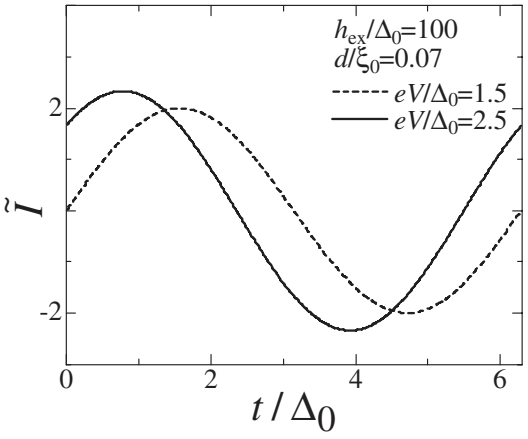

Fig. 6. Ac current $\tilde{I}$ as a function of t/Δ_0 for $h_{ex}/\Delta_0 = 100$, $d/\xi_0 = 0.07$, $eV/\Delta_0 = 1.5$ and 2.5. $\tilde{I} = I\pi e/\sigma_0\Delta_0$.

can confirm the existence of the QPIC when the voltage dependence of the current-phase relation is measured.

4. Summary

In summary, we have studied the ac Josephson effect in the SC/X/SC junction (X = NM, FM). Using a tunneling Hamiltonian and Green's function method, we obtained the Josephson current and the quasiparticle-pair-interference current (QPIC). The Josephson critical current, I_{c1}, shows the Riedel peak at the gap voltage, $V = 2\Delta/e$. In the SC/NM/SC junction, the Riedel peak exhibits weak dependence on d. The amplitude of QPIC, I_{c2}, has a finite value above the gap voltage at $T = 0$ K. These behaviors are similar to those of SC/I/SC junctions. On the other hand, the critical currents in the SC/FM/SC junction show quite different behaviors compared with those in the SC/I/SC and SC/NM/SC junctions. In I_{c1}, the Riedel peak exhibits a strong dependence on d and changes its sign with increasing d due to the 0–π transition. Therefore, at the thickness of the 0–π transition, the Riedel peak disappears. I_{c2} also shows the 0–π transition with increasing d and vanishes at the thickness of the 0–π transition. The ac Josephson current has a strong dependence on the applied voltage, and at the gap voltage the amplitude of I_{c1} shows logarithmic divergence. The amplitude of the higher harmonic Josephson current also shows the applied voltage dependence, similar to the Josephson current. The study of the ac Josephson effect in the SC/FM/SC junction gives a possibility to observe the higher harmonic Josephson current.

We have studied the ferromagnetic Josephson junction in the clean limit in this paper. In many experimental situations, FMs are usually in a diffusive transport region. However, the essence of 0–π transition in the ac Josephson current may be the same even if the case of a dirty FM. Recently, the current–voltage characteristic was studied by using the superconducting phase difference coupled with the spin wave excitation in the ferromagnetic Josephson junction within the phenomenological model.[37] And the dc Josephson current coupled with the spin wave excitation was also discussed.[38] Therefore, it might be important to consider the spin wave excitation for the ac Josephson current from microscopic view point. These problems will be left in a future issue.

Acknowledgments

This work is supported by a Grant-in-Aid for Scientific Research from the Ministry of Education, Culture, Sports, Science and Technology (MEXT), the next Generation Supercomputer Project of MEXT. The authors thank the Supercomputer Center, Institute for Solid State Physics, University of Tokyo for the use of the facilities.

Appendix A: Perturbative Calculation of I_{c1} and I_{c2} in Path Integral Formulation

A.1 Basic formula

In the path integral formulation, the partition function is given by

$$Z = \mathrm{Tr}[\mathrm{e}^{-\beta H}] = \int \mathcal{D}\Psi^* \mathcal{D}\Psi \, \mathrm{e}^{-S} = \int \mathcal{D}\Psi^* \mathcal{D}\Psi \exp\left[-\int_0^\beta \mathrm{d}\tau \left(\int \mathrm{d}r \, \psi^* \partial_\tau \psi + H(\tau)\right)\right], \tag{A·1}$$

where Wick's rotation is performed, $it \to \tau$, $eV/2 \to \mathrm{i}\Omega$ ($\beta = T^{-1}$, τ is an imaginary time variable, Ω is a temporary boson's Matsubara frequency. That becomes $eV/2$ by an analytic continuation.) and $\psi^*\partial_\tau\psi \equiv \psi_{\mathrm{L}}^*\partial_\tau\psi_{\mathrm{L}} + \psi_{\mathrm{FM}}^*\partial_\tau\psi_{\mathrm{FM}} + \psi_{\mathrm{R}}^*\partial_\tau\psi_{\mathrm{R}}$. It is noted that the energy of the left-hand superconductor (L) is different from that of the right-hand superconductor (R), since the voltage, V, is applied. When these systems are separated each other, the time-development in the left-hand side is given by

$$U_{\mathrm{L}}(t,t') = \exp[-\mathrm{i}(H_{\mathrm{L}} - N_{\mathrm{L}})(t-t') + \mathrm{i}(eV/2)N_{\mathrm{L}}(t-t')], \tag{A·2}$$

while that in the right-hand side is

$$U_{\mathrm{R}}(t,t') = \exp[-\mathrm{i}(H_{\mathrm{R}} - N_{\mathrm{R}})(t-t') - \mathrm{i}(eV/2)N_{\mathrm{R}}(t-t')], \tag{A·3}$$

Here, we make a transformation as,

$$\psi_{\mathrm{L}}(\boldsymbol{r},t) = \mathrm{e}^{\mathrm{i}(eV/2)t}\tilde{\psi}_{\mathrm{L}}(\boldsymbol{r},t), \tag{A·4}$$

$$\psi_{\mathrm{R}}(\boldsymbol{r},t) = \mathrm{e}^{-\mathrm{i}(eV/2)t}\tilde{\psi}_{\mathrm{R}}(\boldsymbol{r},t). \tag{A·5}$$

Therefore, H in the action, S, is transformed as

$$\tilde{H}_{\mathrm{BCS}}^{\mathrm{L}} = \sum_\sigma \int \mathrm{d}x \, \tilde{\psi}_{\mathrm{L},\sigma}^* \left(\partial_\tau - \frac{1}{2m}\nabla^2 - \mu\right)\tilde{\psi}_{\mathrm{L},\sigma} - g_{\mathrm{L}} \int \mathrm{d}x \, \tilde{\psi}_{\mathrm{L},\uparrow}^* \tilde{\psi}_{\mathrm{L},\downarrow}^* \tilde{\psi}_{\mathrm{L},\downarrow} \tilde{\psi}_{\mathrm{L},\uparrow}, \tag{A·6}$$

$$\tilde{H}_{\mathrm{FM}} = (\text{unchanged}), \tag{A·7}$$

$$\tilde{H}_{\mathrm{BCS}}^{\mathrm{R}} = (\mathrm{L} \to \mathrm{R}), \tag{A·8}$$

$$\tilde{H}_{\mathrm{T}} = \sum_\sigma \int_{\boldsymbol{r}\in\mathrm{L},\boldsymbol{r}'\in\mathrm{FM}} \mathrm{d}x \, \mathrm{d}x' \, T_{x,x'} \mathrm{e}^{-\mathrm{i}eVt/2} \tilde{\psi}_{\mathrm{L},\sigma}^* \tilde{\psi}_{\mathrm{FM},\sigma} + \sum_\sigma \int_{\boldsymbol{r}\in\mathrm{R},\boldsymbol{r}'\in\mathrm{FM}} \mathrm{d}x \, \mathrm{d}x' \, T_{x,x'} \mathrm{e}^{\mathrm{i}eVt/2} \tilde{\psi}_{\mathrm{R},\sigma}^* \tilde{\psi}_{\mathrm{FM},\sigma} + \mathrm{h.c.} \tag{A·9}$$

For convenience, the tilde is abbreviate: $\tilde{\psi}_{i,\sigma}^{(*)} \equiv \tilde{\psi}_{i,\sigma}^{(*)}(x)$, i is L, R, or FM, $x = (\boldsymbol{r},\tau)$, and $T_{x,x'} \equiv T_{\boldsymbol{r},\boldsymbol{r}'}\delta(\tau-\tau')$. The current operator is defined as

$$\hat{J} = -e\frac{\mathrm{d}N_{\mathrm{L}}}{\mathrm{d}t} = -e\int \mathrm{d}\boldsymbol{r}\frac{\mathrm{d}n_{\mathrm{L}}}{\mathrm{d}t} - \mathrm{i}e\left[\int \mathrm{d}r \, n_{\mathrm{L}}, H\right],$$

$$= -ie \sum_{\sigma} \int_{\boldsymbol{r}\in \mathrm{L}, \boldsymbol{r}'\in \mathrm{FM}} d\boldsymbol{r}\, d\boldsymbol{r}'\, T_{\boldsymbol{r},\boldsymbol{r}'} e^{-ieVt/2} \psi^{\dagger}_{\mathrm{L},\sigma} \psi_{\mathrm{FM},\sigma} + \mathrm{h.c.}, \tag{A·10}$$

$$n_{\mathrm{L}} = \sum_{\sigma} \psi^{\dagger}_{\mathrm{L},\sigma} \psi_{\mathrm{L},\sigma}. \tag{A·11}$$

We eliminate the quartic interaction term in Hamiltonian eqs. (A·6) and (A·8) using Stratonovich–Hubbard transformation,

$$1 = \int \mathcal{D}\Delta^* \mathcal{D}\Delta \times \exp\left[-\frac{1}{g} \int dx (\Delta - g\psi_{\downarrow}\psi_{\uparrow})(\Delta^* - g\psi^*_{\uparrow}\psi^*_{\downarrow}) \right], \tag{A·12}$$

where $\Delta^{(*)} \equiv \Delta^{(*)}(x)$. With this transformation, the action becomes

$$S = S_{\mathrm{cond}} + S_{\mathrm{el}}, \tag{A·13}$$

$$S_{\mathrm{cond}} = \int dx \frac{|\Delta_{\mathrm{L}}|^2}{g_{\mathrm{L}}} + \int dx \frac{|\Delta_{\mathrm{R}}|^2}{g_{\mathrm{R}}}, \tag{A·14}$$

$$S_{\mathrm{el}} = \int dx \int dx'\, \Psi^*(x)[G^-]\Psi(x'). \tag{A·15}$$

The Green's function, $G^- \equiv G^-(x,x')$, is a 6×6 matrix spanned both in the space of L, FM, R, and Nambu space. The electronic fields are expressed as

$$\Psi(x) \equiv \begin{pmatrix} \psi_{\mathrm{L}\uparrow} \\ \psi^*_{\mathrm{L}\downarrow} \\ \psi_{\mathrm{FM}\uparrow} \\ \psi^*_{\mathrm{FM}\downarrow} \\ \psi_{\mathrm{R}\uparrow} \\ \psi^*_{\mathrm{R}\downarrow} \end{pmatrix}, \tag{A·16}$$

The inverse of the Green's function for electron system, G^-, is given by

$$\hat{G}^- = \begin{bmatrix} -\hat{G}^-_{\mathrm{L}} & \hat{T} & 0 \\ \hat{T}^* & -\hat{G}^-_{\mathrm{FM}} & \hat{T} \\ 0 & \hat{T}^* & -\hat{G}^-_{\mathrm{R}} \end{bmatrix} = -\hat{G}^-_0 + \hat{\mathrm{P}}, \tag{A·17}$$

$$-\hat{G}^{-1}_0 = \begin{bmatrix} -\hat{G}^-_{\mathrm{L}} & 0 & 0 \\ 0 & -\hat{G}^-_{\mathrm{FM}} & 0 \\ 0 & 0 & -\hat{G}^-_{\mathrm{R}} \end{bmatrix}, \tag{A·18}$$

$$\hat{\mathrm{P}} = \begin{bmatrix} 0 & \hat{T} & 0 \\ \hat{T}^* & 0 & \hat{T} \\ 0 & \hat{T}^* & 0 \end{bmatrix}, \tag{A·19}$$

$$-\hat{G}^-_{\mathrm{L}} = \left[\partial_\tau \hat{\sigma}_0 - \left(\frac{1}{2m}\Delta + \mu \right)\hat{\sigma}_3 - \Delta_{\mathrm{L}} e^{i\theta_{\mathrm{L}}\hat{\sigma}_3}\hat{\sigma}_1 \right] \times \delta(x-x'), \tag{A·20}$$

$$-\hat{G}^-_{\mathrm{R}} = (\mathrm{L}\to\mathrm{R}), \tag{A·21}$$

$$-\hat{G}^-_{\mathrm{FM}} = \left[\partial_\tau \hat{\sigma}_0 - \left(\frac{1}{2m}\Delta + \mu + i\sigma h_{\mathrm{ex}} \right)\hat{\sigma}_3 \right] \times \delta(x-x'), \tag{A·22}$$

$$\hat{T} = \begin{bmatrix} e^{-i\Omega\tau} T_{\boldsymbol{r},\boldsymbol{r}'} & 0 \\ 0 & -e^{i\Omega\tau} T^*_{\boldsymbol{r},\boldsymbol{r}'} \end{bmatrix} \delta(\tau - \tau'). \tag{A·23}$$

$\hat{\sigma}_1$, $\hat{\sigma}_3$ are the Pauli matrices and $\hat{\sigma}_0$ is a unit matrix. $\theta_{\mathrm{L(R)}}$ is the phase of superconducting order parameter, $\Delta_{\mathrm{L(R)}} e^{i\theta_{\mathrm{L(R)}}}$. Below, we consider the case that the superconductor L and R are same.

An auxiliary field, ϕ, that couples to the current operator, $\hat{J}$, is introduced in eq. (A·10) as,

$$S_{\mathrm{cond}} = \int dx \frac{|\Delta_{\mathrm{L}}|^2}{g_{\mathrm{L}}} + \int dx \frac{|\Delta_{\mathrm{R}}|^2}{g_{\mathrm{R}}} + \int_0^\beta d\tau\, \phi J, \tag{A·24}$$

$$\phi J = \phi \int dx\, dx'\, \Psi^*(x)[\hat{J}]\Psi(x'), \tag{A·25}$$

where $\phi \equiv (\tau)$ and $J \equiv J(x,x')$. The current operator is denoted as,

$$\hat{J} = \begin{bmatrix} 0 & -ie\hat{R} & 0 \\ ie\hat{R}^* & 0 & 0 \\ 0 & 0 & 0 \end{bmatrix}, \tag{A·26}$$

$$\hat{R} = \begin{bmatrix} e^{-i\Omega\tau} T_{\boldsymbol{r},\boldsymbol{r}'} & 0 \\ 0 & e^{i\Omega\tau} T^*_{\boldsymbol{r},\boldsymbol{r}'} \end{bmatrix} \delta(\tau - \tau'). \tag{A·27}$$

Tracing out the electron fields from eq. (A·25), we obtain the effective free energy, F_{eff}, with Josephson junction as following,

$$\beta F_{\mathrm{eff}} = -\mathrm{Tr}\{\ln[\hat{G}^{-1} + \phi\hat{J}]\} = -\mathrm{Tr}\{\ln[(-\hat{G}^-_0 + \phi\hat{J}) + \hat{\mathrm{P}}]\}. \tag{A·28}$$

In eq. (A·28), Tr means taking trace with respect to the matrix element of the Green's function and integrating with respect to x, x'. In the fourth order perturbation theory about the tunneling matrix, the current is approximated to be

$$\langle J \rangle = \frac{\partial F_{\mathrm{eff}}}{\partial \phi}\bigg|_{\phi=0} = -\frac{1}{\beta}\frac{\partial}{\partial\phi}\mathrm{Tr}\{\ln[(-\hat{G}^-_0 + \phi\hat{J}) + \hat{\mathrm{P}}]\}\bigg|_{\phi=0} \simeq \frac{1}{\beta}\mathrm{Tr}[\hat{J}\hat{G}_0] + \frac{1}{\beta}\mathrm{Tr}[\hat{J}\hat{G}_0\hat{\mathrm{P}}\hat{G}_0] + \frac{1}{\beta}\mathrm{Tr}[\hat{J}\hat{G}_0\hat{\mathrm{P}}\hat{G}_0\hat{\mathrm{P}}\hat{G}_0\hat{\mathrm{P}}\hat{G}_0]. \tag{A·29}$$

The first and second terms does not contribute the Josephson current, whose leading term is the third one in eq. (A·29).

Because Tr is not affected by a change of basis, the matrix element can be transformed from $(\boldsymbol{r},\tau)$ component to its Fourier component $(\boldsymbol{k}, i\omega_n)$. Here, $i\omega_n$ is the Matsubara frequency of the electrons. Here we made use of the fact that the tunneling matrix element differs from 0 only for $\boldsymbol{r}\sim\boldsymbol{r}'$ and in the neighborhood of the SC/FM boundary, i.e., $T_{\boldsymbol{r},\boldsymbol{r}'} = T_0\delta(\boldsymbol{r}-\boldsymbol{r}')\delta(\boldsymbol{r}-\boldsymbol{r}_{\mathrm{L(R)}})$, where $\boldsymbol{r}_{\mathrm{L(R)}}$ is the position of the interface between the left (right) SC and the FM. Tracing out the matrix element of the Green's function, we can obtain the current formula as follows,

$$I_{\mathrm{J}} = -8eT_0^4\,\mathrm{Im}\frac{1}{\beta} \times \sum_{\{k\}, i\omega_n} [e^{i(\boldsymbol{k}^{\uparrow}_{\mathrm{FM}} - \boldsymbol{k}^{\downarrow}_{\mathrm{FM}})\boldsymbol{r}} f_{\mathrm{L}}(\boldsymbol{k}_{\mathrm{L}}, i\omega_n + i\Omega) g^{(0)}_{\mathrm{FM},\uparrow}(\boldsymbol{k}^{\uparrow}_{\mathrm{FM}}, i\omega_n) \times g^{(0)}_{\mathrm{FM},\downarrow}(\boldsymbol{k}^{\downarrow}_{\mathrm{FM}}, -i\omega_n) f^*_{\mathrm{R}}(\boldsymbol{k}_{\mathrm{R}}, i\omega_n - i\Omega)], \tag{A·30}$$

where $\boldsymbol{r} = \boldsymbol{r}_{\mathrm{R}} - \boldsymbol{r}_{\mathrm{L}}$ and each Green's function is given by

$$f_{\mathrm{L}}(\boldsymbol{k}_{\mathrm{L}}, i\omega_n + i\Omega) = \frac{\Delta_{\mathrm{L}} e^{i\varphi_{\mathrm{L}}}}{(\omega_n + \Omega)^2 + \xi^2_{\mathrm{L}} + \Delta^2_{\mathrm{L}}}, \tag{A·31}$$

$$f_{\mathrm{R}}(\boldsymbol{k}_{\mathrm{L}}, \mathrm{i}\omega_n - \mathrm{i}\Omega) = (\mathrm{L} \to \mathrm{R}), \tag{A·32}$$

$$g^{(0)}_{\mathrm{FM},\uparrow}(\boldsymbol{k}_{\mathrm{FM}\uparrow}, \mathrm{i}\omega_n) = -\frac{1}{\mathrm{i}\omega_n - \xi^{\uparrow}_{\mathrm{FM}}}, \tag{A·33}$$

$$g^{(0)}_{\mathrm{FM},\downarrow}(-\boldsymbol{k}_{\mathrm{FM}\downarrow}, -\mathrm{i}\omega_n) = -\frac{1}{\mathrm{i}\omega_n + \xi^{\downarrow}_{\mathrm{FM}}}, \tag{A·34}$$

$$\xi_{\mathrm{L(R)}} = \frac{k^2_{\mathrm{L(R)}}}{2m} - \mu, \tag{A·35}$$

$$\xi^{\sigma}_{\mathrm{FM}} = \frac{k^2_{\mathrm{FM}}}{2m} - \mu - \sigma h_{\mathrm{ex}}. \tag{A·36}$$

Note that $k_{\mathrm{FM}\uparrow}$ and $k_{\mathrm{FM}\downarrow}$ are independent of each other. After integrating Green's functions of the FM as to $k_{\mathrm{FM},\sigma}$, we can obtain the following formula,

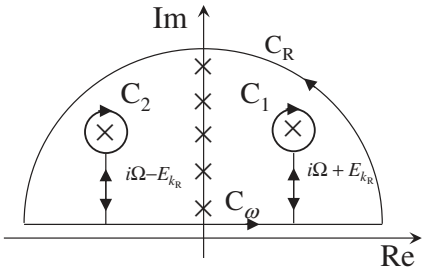

Fig. B·1. Paths in the complex plane for the contour integration of eq. (B·1).

$$\begin{aligned} I_{\mathrm{J}} &= 16eT_0^4\left[\frac{mv}{2\pi d}\right]^2 \mathrm{Im}\left[\mathrm{i}\frac{\Delta^2}{\beta}\sum_{k_{\mathrm{L}},k_{\mathrm{R}},\omega_n>0}\frac{1}{(\omega_n+\Omega)^2+E^2_{k_{\mathrm{L}}}}\frac{1}{(\omega_n-\Omega)^2+E^2_{k_{\mathrm{R}}}}\cos\left(\frac{2h_{\mathrm{ex}}}{v_{\mathrm{F}}d}\right)\mathrm{e}^{-2\omega_n d/v_{\mathrm{F}}}\right]\sin\theta \\ &\quad + 16eT_0^4\left[\frac{mv}{2\pi d}\right]^2 \mathrm{Im}\left[\frac{\Delta^2}{\beta}\sum_{k_{\mathrm{L}},k_{\mathrm{R}},\omega_n>0}\frac{1}{(\omega_n+\Omega)^2+E^2_{k_{\mathrm{L}}}}\frac{1}{(\omega_n-\Omega)^2+E^2_{k_{\mathrm{R}}}}\cos\left(\frac{2h_{\mathrm{ex}}}{v_{\mathrm{F}}d}\right)\mathrm{e}^{-2\omega_n d/v_{\mathrm{F}}}\right]\cos\theta \\ &\equiv I_{\mathrm{c1}}\sin\theta + I_{\mathrm{c2}}\cos\theta, \end{aligned} \tag{A·37}$$

where v is a volume of the FM, k_{F} is the Fermi wave number, $\beta = T^{-1}$.

Appendix B: Summation of Matsubara Frequency

We evaluate Matsubara frequency summation in (A·37). This summation is performed by a contour integration in Fig. B·1. The integral has the form

$$I_{\mathrm{C}} = -\oint_{\mathrm{C}}\frac{\mathrm{d}z}{2\pi i}f(z)n_{\mathrm{F}}(z)\mathrm{e}^{\mathrm{i}2zd/v_{\mathrm{F}}}, \tag{B·1}$$

$$f(z) = \frac{1}{z+\mathrm{i}\Omega-E_{k_{\mathrm{L}}}}\frac{1}{z+\mathrm{i}\Omega+E_{k_{\mathrm{L}}}}\frac{1}{z-\mathrm{i}\Omega-E_{k_{\mathrm{R}}}}\frac{1}{z-\mathrm{i}\Omega+E_{k_{\mathrm{R}}}}, \tag{B·2}$$

$$\mathrm{C} = \mathrm{C}_1 + \mathrm{C}_2 + \mathrm{C}_\omega + \mathrm{C}_R, \tag{B·3}$$

where $n_{\mathrm{F}}(z)$ is a Fermi distribution function, C_1 and C_2 are a closed path enclosing the pole of the anomalous Green's function, C_ω is a integration on the real axis of complex plane, and C_R is a large semicircle of radius R in the limit as $R \to \infty$. The contour integration with C_R is zero because of the Jordan's theorem. When each contour integration is performed, the following result is obtained,

$$I_{\mathrm{C1}} = \frac{1}{4E_{k_{\mathrm{L}}}E_{k_{\mathrm{R}}}}\left(\frac{1}{\mathrm{i}2\Omega+E_{k_{\mathrm{R}}}-E_{k_{\mathrm{L}}}} - \frac{1}{\mathrm{i}2\Omega+E_{k_{\mathrm{R}}}-E_{k_{\mathrm{L}}}}\right)n_{\mathrm{F}}(E_{k_{\mathrm{R}}})\exp\left(\mathrm{i}\frac{\mathrm{i}2\Omega+2E_{k_{\mathrm{R}}}}{v_{\mathrm{F}}}d\right) \tag{B·4}$$

$$I_{\mathrm{C2}} = -\frac{1}{4E_{k_{\mathrm{L}}}E_{k_{\mathrm{R}}}}\left(\frac{1}{\mathrm{i}2\Omega-E_{k_{\mathrm{R}}}-E_{k_{\mathrm{L}}}} - \frac{1}{\mathrm{i}2\Omega-E_{k_{\mathrm{R}}}+E_{k_{\mathrm{L}}}}\right)n_{\mathrm{F}}(-E_{k_{\mathrm{R}}})\exp\left(\mathrm{i}\frac{\mathrm{i}2\Omega-2E_{k_{\mathrm{R}}}}{v_{\mathrm{F}}}d\right) \tag{B·5}$$

$$\begin{aligned} I_\omega = \Bigg[&-\int_{-\infty}^{\infty}\frac{\mathrm{d}\omega}{\pi\mathrm{i}}\frac{1}{4E_{k_{\mathrm{L}}}E_{k_{\mathrm{R}}}}\frac{1}{\mathrm{i}2\Omega-E_{k_{\mathrm{R}}}-E_{k_{\mathrm{L}}}}\left(\frac{1}{\mathrm{i}2\Omega+2\omega-2E_{k_{\mathrm{L}}}}+\frac{1}{\mathrm{i}2\Omega-2\omega-2E_{k_{\mathrm{R}}}}\right) \\ &+\int_{-\infty}^{\infty}\frac{\mathrm{d}\omega}{\pi\mathrm{i}}\frac{1}{4E_{k_{\mathrm{L}}}E_{k_{\mathrm{R}}}}\frac{1}{\mathrm{i}2\Omega+E_{k_{\mathrm{R}}}-E_{k_{\mathrm{L}}}}\left(\frac{1}{\mathrm{i}2\Omega+2\omega-2E_{k_{\mathrm{L}}}}+\frac{1}{\mathrm{i}2\Omega-2\omega+2E_{k_{\mathrm{R}}}}\right) \\ &+\int_{-\infty}^{\infty}\frac{\mathrm{d}\omega}{\pi\mathrm{i}}\frac{1}{4E_{k_{\mathrm{L}}}E_{k_{\mathrm{R}}}}\frac{1}{\mathrm{i}2\Omega-E_{k_{\mathrm{R}}}+E_{k_{\mathrm{L}}}}\left(\frac{1}{\mathrm{i}2\Omega+2\omega+2E_{k_{\mathrm{L}}}}+\frac{1}{\mathrm{i}2\Omega-2\omega-2E_{k_{\mathrm{R}}}}\right)n_{\mathrm{F}}(\omega)\exp\left(\mathrm{i}\frac{\omega}{\mu}k_{\mathrm{F}}L\right) \end{aligned} \tag{B·6}$$

$$-\int_{-\infty}^{\infty}\frac{\mathrm{d}\omega}{\pi\mathrm{i}}\frac{1}{4E_{k_{\mathrm{L}}}E_{k_{\mathrm{R}}}}\frac{1}{\mathrm{i}2\Omega+E_{k_{\mathrm{R}}}+E_{k_{\mathrm{L}}}}\left(\frac{1}{\mathrm{i}2\Omega+2\omega+2E_{k_{\mathrm{L}}}}+\frac{1}{\mathrm{i}2\Omega-2\omega+2E_{k_{\mathrm{R}}}}\right)\Bigg]n_{\mathrm{F}}(\omega)\exp\left(\mathrm{i}\frac{2\omega}{v_{\mathrm{F}}}d\right). \tag{B·7}$$

Here, we consider the case of absolute zero temperature. Then $n_{\mathrm{F}}(E_{k_{\mathrm{L(R)}}}) = 0$, $n_{\mathrm{F}}(\omega) = \Theta(-\omega)$. Making an analytic continuation $\mathrm{i}2\Omega \to eV + \mathrm{i}\delta$ and integrations with respect to ω and $E_{k_{\mathrm{L}}}$ or $E_{k_{\mathrm{R}}}$, we obtain the analytical form of I_{c1} and I_{c2},

$$\begin{aligned} I_{\mathrm{c1}} = \frac{\sigma_0\Delta_0^2}{\pi e}\int_{\Delta_0}^{\infty}\mathrm{d}E\,\frac{\Theta(\Delta_0-|E-eV|)}{\sqrt{E^2-\Delta_0^2}\sqrt{\Delta_0^2-(E-eV)^2}}\Bigg\{&\mathrm{Ci}\left(\frac{2E-eV}{v_{\mathrm{F}}}d\right)\sin\left(\frac{2E-eV}{v_{\mathrm{F}}}d\right) \\ &-\cos\left(\frac{2E-eV}{v_{\mathrm{F}}}d\right)\left[\mathrm{Si}\left(\frac{2E-eV}{v_{\mathrm{F}}}d\right)-\frac{\pi}{2}\right]\Bigg\}\cos\left(\frac{2h_{\mathrm{ex}}}{v_{\mathrm{F}}}d\right), \end{aligned} \tag{B·8}$$

$$I_{c2} = \frac{\sigma_0 \Delta_0^2}{e} \int_0^{eV/2-\Delta_0} dE \frac{\Theta(eV - 2\Delta_0)}{\sqrt{(E + eV/2)^2 - \Delta_0^2}\sqrt{(E - eV/2)^2 - \Delta_0^2}} \cos\left(\frac{2E}{v_F} d\right) \cos\left(\frac{2h_{ex}}{v_F} d\right), \quad \text{(B·9)}$$

where $\sigma_0 = 16\pi e^2 T_0^4 N_L(0) N_R(0) [mv/(2\pi d)]^2$.

1) B. D. Josephson: Phys. Lett. **1** (1962) 251.
2) E. Riedel: Z. Naturforsch. A **19** (1964) 1634.
3) N. R. Werthamer: Phys. Rev. **147** (1966) 255.
4) A. C. Hamilton and S. Shapiro: Phys. Rev. Lett. **26** (1971) 426.
5) R. E. Harris: Phys. Rev. B **10** (1974) 84.
6) S. A. Buckner and D. N. Langenberg: J. Low Temp. Phys. **22** (1976) 569.
7) S. Morita, S. Imai, I. Fukushi, S. Takaki, Y. Takeuti, and N. Mikoshiba: J. Phys. Soc. Jpn. **52** (1983) 617.
8) O. H. Soerensen, J. Mygind, and N. F. Pedersen: Phys. Rev. Lett. **39** (1977) 1018.
9) K. K. Likharev: Rev. Mod. Phys. **51** (1979) 101.
10) D. Averin and A. Bardas: Phys. Rev. Lett. **75** (1995) 1831.
11) M. Hurd, S. Datta, and F. Bagwell: Phys. Rev. B **56** (1997) 11232.
12) R. S. Gonnelli, A. Calzolari, D. Daghero, and G. A. Ummarino: Phys. Rev. Lett. **87** (2001) 97001.
13) Q. Sun, H. Guo, and J. Wang: Phys. Rev. B **65** (2002) 075315.
14) A. Jacobs and R. Kümmel: Phys. Rev. B **71** (2005) 184504.
15) A. A. Golubov, M. Yu. Kupriyanov, and E. Ilfichev: Rev. Mod. Phys. **76** (2004) 411.
16) A. I. Buzdin: Rev. Mod. Phys. **77** (2005) 935.
17) V. V. Ryazanov, V. A. Oboznov, A. Yu. Rusanov, A. V. Veretennikov, A. A. Golubov, and J. Aarts: Phys. Rev. Lett. **86** (2001) 2427.
18) T. Kontos, M. Aprili, J. Lesueur, F. Genet, B. Stephanidis, and R. Boursier: Phys. Rev. Lett. **89** (2002) 137007.
19) H. Sellier, C. Baraduc, F. Lefloch, and R. Calemczuk: Phys. Rev. B **68** (2003) 054531.
20) H. Sellier, C. Baraduc, F. Lefloch, and R. Calemczuk: Phys. Rev. Lett. **92** (2004) 257005.
21) A. Bauer, J. Bentner, M. Aprili, M. L. Della Rocca, M. Reinwald, W. Wegscheider, and C. Strunk: Phys. Rev. Lett. **92** (2004) 217001.
22) S. M. Frolov, D. J. Van Harlingen, V. A. Oboznov, V. V. Bolginov, and V. V. Ryazanov: Phys. Rev. B **70** (2004) 144505.
23) C. Bell, R. Loloee, G. Burnell, and M. G. Blamire: Phys. Rev. B **71** (2005) 180501.
24) F. Born, M. Siegel, E. K. Hollmann, H. Braak, A. A. Golubov, D. Yu. Gusakova, and M. Yu. Kupriyanov: Phys. Rev. B **74** (2006) 140501.
25) M. Weides, M. Kemmler, H. Kohlstedt, R. Waser, D. Koelle, R. Kleiner, and E. Goldobin: Phys. Rev. Lett. **97** (2006) 247001.
26) V. A. Oboznov, V. V. Bol'ginov, A. K. Feofanov, V. V. Ryazanov, and A. I. Buzdin: Phys. Rev. Lett. **96** (2006) 197003.
27) V. Shelukhin, A. Tsukernik, M. Karpovski, Y. Blum, K. B. Efetov, A. F. Volkov, T. Champel, M. Eschrig, T. Löfwander, G. Schon, and A. Palevski: Phys. Rev. B **73** (2006) 174506.
28) M. Mori, S. Hikino, S. Takahashi, and S. Maekawa: J. Phys. Soc. Jpn. **76** (2007) 054705.
29) P. Fulde and R. Ferrell: Phys. Rev. **135** (1964) A550.
30) A. I. Larkin and Y. N. Ovchinnikov: Zh. Eskp. Teor. Fiz. **47** (1964) 1136 [Sov. Phys. JETP **20** (1965) 762].
31) T. Yamashita, K. Tanikawa, S. Takahashi, and S. Maekawa: Phys. Rev. Lett. **95** (2005) 097001.
32) T. Yamashita, S. Takahashi, and S. Maekawa: Appl. Phys. Lett. **88** (2006) 132501.
33) L. G. Aslamazov, A. I. Larkin, and Y. N. Ovchinnikov: Sov. Phys. JETP **28** (1969) 171.
34) K. Awaka and H. Fukuyama: J. Phys. Soc. Jpn. **66** (1997) 2820.
35) R. Melin: Europhys. Lett. **69** (2005) 121.
36) A. Barone and G. Paternò: *Physics and Applications of the Josephson Effect* (Wiley, New York, 1982).
37) S. Hikino, M. Mori, S. Takahashi, and S. Maekawa: J. Phys. Soc. Jpn. **77** (2008) 053707.
38) M. Houzet: Phys. Rev. Lett. **101** (2008) 057009.